Cite this article as: Ganne A., et al. (2024). Ezetimibe Lowers Risk of Alzheimer's and Related Dementias over Sevenfold, Reducing Aggregation in Model Systems by Inhibiting 14-3-3G::Hexokinase Interaction, *AgingBio*, *2*, e20240028. doi: 10.59368/agingbio.20240028.

Research Paper

Ezetimibe Lowers Risk of Alzheimer's and Related Dementias over Sevenfold, Reducing Aggregation in Model Systems by Inhibiting 14-3-3G::Hexokinase Interaction

Akshatha Ganne,[1] Nirjal Mainali,[1,2] Meenakshisundaram Balasubramaniam,[1,3] Ramani Atluri,[1,3] Sonu Pahal,[1,2] Joseph J. Asante,[1,2] Corey Nagel,[4] Srikanth Vallurupalli,[3,5] Robert J. Shmookler Reis,[1,2,3,6,*] and Srinivas Ayyadevara[1,2,3,6,*]

[1]Department of Geriatrics and Institute on Aging, University of Arkansas for Medical Sciences, Little Rock, AR, USA
[2]Bioinformatics Program, University of Arkansas at Little Rock and University of Arkansas for Medical Sciences, Little Rock, AR, USA
[3]Central Arkansas Veterans Healthcare System, Little Rock, AR, USA
[4]College of Nursing, University of Arkansas for Medical Sciences, Little Rock, AR, USA
[5]Department of Internal Medicine, Division of Cardiology, University of Arkansas for Medical Sciences, Little Rock, AR, USA
[6]Geriatric Research Education and Clinical Center (GRECC), Veterans Healthcare Administration, Little Rock, AR, USA
[*]Corresponding authors: rjsr@uams.edu; AyyadevaraSrinivas@uams.edu
https://doi.org/10.59368/agingbio.20240028
Received: 4/22/2024, Revised: 5/1/2024, Accepted: 5/13/2024, Published: 6/26/2024

Numerous factors predispose to the progression of cognitive impairment to Alzheimer's disease and related dementias (ADRD), most notably age, *APOE*(ϵ4) alleles, traumatic brain injury, heart disease (HtD), hypertension, obesity/diabetes, and Down's syndrome. Protein aggregation is diagnostic for neurodegenerative diseases and may be causal through the promotion of chronic neuroinflammation. We isolated aggregates from postmortem hippocampi of ADRD patients, HtD patients, and age-matched controls. Aggregates, characterized by high-resolution proteomics (with or without cross-linking), were significantly elevated in HtD and ADRD hippocampi. Hexokinase-1 (HK1) and 14-3-3G/γ proteins, previously implicated in neuronal signaling and neurodegeneration, are especially enriched in ADRD and HtD aggregates versus controls (each $P < 0.008$), and their interaction was implied by extensive cross-linking in both disease groups. Screening the HK1::14-3-3G interface with structures of drugs approved by the U.S. Food and Drug Administration (FDA) predicted strong affinity for ezetimibe, a benign cholesterol-lowering medication. Diverse cultured human-cell and whole-nematode models of ADRD aggregation showed that this drug potently disrupts HK1::14-3-3G adhesion, reduces disease-associated aggregation, and activates autophagy. Mining clinical databases supports drug reduction of ADRD risk, decreasing it to 0.14 overall ($P < 0.0001$; 95% C.I. 0.06–0.34) and <0.12 in high-risk HtD subjects ($P < 0.006$). These results suggest that drug disruption of the 14-3-3G::HK1 interface blocks an early "lynchpin" adhesion, prospectively reducing aggregate accrual and progression of ADRD.

Introduction

Neurodegenerative diseases, of which Alzheimer's disease (AD) is the most prevalent form, are debilitating and costly in terms of both human suffering and health-care costs[1]. Aging is the most important risk factor for AD onset and progression, although genetic factors (*APOE[ϵ4]* alleles or Down's syndrome) also confer high susceptibility. Other predisposing conditions include traumatic brain injury, coronary artery disease (CAD) and other heart disease (HtD), hypertension, obesity/diabetes, and smoking[2,3]. Most, if not all, of these predispositions are reflected in the burden of aggregate accumulation in the brain, in particular the hippocampus. Both AD and HtD elevate aggregate load in human hippocampi[4,5], but our most compelling evidence comes from studies of mouse models that simulate many of the above risk factors. Experimentally induced hypertension[6], myocardial infarction[5], and traumatic brain injury[7], as well as diet-induced obesity[8] and aging[6,9–11], are all associated with increased accrual of protein aggregates in humans and model organisms, and interventions which mitigate that accrual confer protection from cognitive impairment[12–15]. Mouse models have been developed that exacerbate the normal, age-progressive growth of cerebral aggregates, producing deficits in cognition and learning[16,17]. A mechanistic link between aggregation and dementia, although unproven, is supported by the strong negative correlation between aggregate burden and cognitive performance[18,19].

Hexokinase-1 (HK1) and multiple 14-3-3 paralogs have been implicated in cancer, aging, and neurodegenerative diseases, including AD[12,20–24]. Expression of the 14-3-3 protein family is altered during aging and in age-related diseases such as

AD[20,22,25]. Pathways that influence protein homeostasis, including autophagy, are positively regulated by 14-3-3 proteins[26,27]. Decreased glucose metabolism is a significant contributor to AD pathogenesis[28,29], and the expression and activity of hexokinase, the rate-limiting enzyme of glucose metabolism, are reduced in AD brain, fibroblasts, leukocytes, and microvessels[24].

HK-1 is normally associated with the mitochondrial outer membrane, but in AD it disassociates from mitochondria, leading to the release of interleukin IL-1β, activation of inflammasomes, and apoptosis of neurons[30,31]. Accumulation of amyloid β in plaque[32] and formation of α-synuclein fibers[23] were found to stimulate HK-1 release from the mitochondrial outer membrane, causing it to depolarize; moreover, HK-1 expression increases after a reduction of IL-1β levels[31]. Synthetic HK1 peptides improve mitochondrial function in a cell-culture model of ALS[33]. We reported increased accumulation of both 14-3-3 and HK1 in detergent-insoluble aggregates, while protein–protein interaction (PPI) inhibitors disrupting these interactions reduce protein aggregation and improve physiological function in AD models[12].

We focus here on the well-documented AD risk elevation among HtD patients[34,35], estimated to confer a 1.4–1.9 relative risk (RR) for AD[36,37] (see also **Tables 2** and **3**). Remarkably, hippocampi from HtD patients display a >50% increase in their aggregate load relative to age-matched controls (AMCs; this study). Constituent proteins of these aggregates overlap substantially with those from AD brains, suggesting that HtD may promote AD onset by the same mechanisms through which aging favors AD.

Methods and Materials

C. elegans strains

All nematodes were cultured using standard methods as previously described[9,12]. Strains were maintained at 20°C on 2% (w/v) agar plates incorporating nematode growth medium[12] and covered with a central lawn of *E. coli* strain OP50, unless otherwise specified. This study employed *C. elegans* strains MT14355, carrying a 14-3-3 (*ftt-2*) deletion (*ftt-2*[n4426 X]); UA57, expressing GFP in dopaminergic neurons *[baIs4 (Pdat-1::GFP, Pdat-1::CAT-2)]*; VH255, expressing tau in body-wall muscle [hdEx82 (F25B3.3::tau3529WT)+*pha-1*(+)] and becoming paralyzed with age; and CL2355 (*dvIs50*[*pCL45*(*snb-1::Aβ1–42::3′* UTR (long)+*mtl-2::GFP*]), a model of amyloid deposition with pan-neuronal expression of human $A\beta_{1-42}$ peptide. These strains were all provided by the Caenorhabditis Genetics Center (Minneapolis, MN, USA). Strain UA355 (*baIn51* [P_{eat-4}::*APOEε4*, P_{unc-54}::*tdTomato*]; *baIn34* [P_{eat-4}::*Aβ*, P_{myo-2}::*mCherry*]; *adIs1240* [P_{eat-4}::*GFP*]) was a gift from Drs. Guy and Kim Caldwell (University of Alabama).

Nematode culture

C. elegans were grown at 20°C on 100-mm NGM-agar Petri dishes seeded with a central lawn of *E. coli* (strain OP50) and either ezetimibe or dimethyl sulfoxide (DMSO) vehicle for control plates. Gravid young-adult worms were lysed, releasing unlaid eggs to initiate a synchronized-aging cohort. Equal numbers of eggs were placed on each plate.

Chemotaxis of transgenic *C. elegans* expressing neuronal $A\beta_{1-42}$ peptide

C. elegans strain CL2355, expressing human $A\beta_{1-42}$ in all neurons, were aged to adult day 5 at 20°C. Chemotaxis to n-butanol was assayed as described previously[4,12].

Paralysis assay in a transgenic *C. elegans* strain expressing human tau in muscle

Cohorts of *C. elegans* strain VH255, expressing human tau in muscle, were maintained as described above, with or without ezetimibe; paralyzed and motile worms were counted on days 8 and 13 post-hatch.

Neuronal degeneration assay

Synchronized cohorts of strain UA57 worms, expressing Green Fluorescent Protein (GFP) in all dopaminergic neurons, were maintained as described above, with or without 10-μM ezetimibe. Surviving neurons were visualized and quantified by GFP fluorescence.

Ezetimibe treatment of cultured human cell lines

Cultures of SH-SY5Y-APP_{Sw} (neuroblastoma cells expressing a familial-AD mutant of amyloid precursor protein), HEK-tau (human embryonic kidney cells overexpressing tau), and SY5Y-tau (human neuroblastoma cells overexpressing tau) were maintained in exponential growth at 37°C in DMEM + F12 (Life Technologies; Carlsbad, CA, USA) supplemented with 10% (v/v) Fetal Bovine Serum. Cells were trypsinized and replated at 5,000–-10,000 cells/well in 96-well plates and grown 16 hours at 37°C as above. Ezetimibe or vehicle was added to cultures at ~40% confluence, and cells were fixed in 4% formaldehyde after 48 hours, stained with 0.1% w/v Thioflavin T, washed 4×, and aggregation was quantified by fluorescence, imaging 9 fields per well. Thioflavin T (green) fluorescence was divided by the number of DAPI-stained nuclei per field to obtain normalized values (amyloid per cell), summarized as means ± SEM (standard error of the mean).

Quantitation of autophagy

SY5Y-APP_{Sw} neuroblastoma cells were plated at 10,000 cells per well in eight-chambered slides. Ezetimibe or vehicle (control) was added after 16 hours, and autophagy was assessed 48 hours later using an Autophagy Assay Kit (ab139484, Abcam). A Keyence™ microscope allowed automated quantitation of FITC (green) fluorescence and counting of DAPI-stained nuclei (blue) per field.

Isolation of protein aggregates

Human hippocampi and pellets of *C. elegans* strain MT14355 (14-3-3/*ftt-2* deletion) were flash-frozen in liquid nitrogen and homogenized at 0°C in buffer containing 1% v/v NP40, 20-mM HEPES (pH 7.4), 300-mM NaCl, 2-mM $MgCl_2$, and protease/phosphatase inhibitors (CalBiochem; San Diego, CA). Lysates were centrifuged (2000 rpm; 492 × g) for 5 min at 4°C to remove debris, and supernatants were sonicated to disrupt cells and membrane-bound organelles. Protein was quantified with Bradford reagent (Bio-Rad; Hercules, CA, USA), and 1.0-mg aliquots were incubated for 12 hours with 14-3-3 antibody-coated Dynabeads™ (MA5-12242, ThermoFisher). Bound proteins were recovered, suspended in 0.1-M HEPES (pH 7.4) containing 1% v/v sarcosyl and 5-mM EDTA, and centrifuged for 30 min at 100,000 × g. Pellets (sarkosyl-insoluble proteins) were resuspended by boiling for 5 min in Laemmli buffer containing 50-mM dithiothreitol and 2% v/v sodium dodecyl sulfate (SDS) and resolved by electrophoresis on 4%–20% polyacrylamide gradient gels containing 1% w/v SDS. Gels were stained with SYPRO-Ruby (ThermoFisher; Waltham, MA, USA) to visualize and quantify protein.

Source metadata for human hippocampal tissue

Human hippocampi were obtained from the UAMS Brain Bank (maintained by Dr. Sue T. Griffin), where they have been stored at −80°C following postmortem dissection.

Metadata for the tissue-source patients are as follows:

	Age	Race/Sex	*APOE* Genotype
AMC 1	69	White male	3,3
AMC 2	83	White male	3,3
AMC 3	80	White male	3,3
Mean AMC age	77.3		
AD 1	74	White male	4,4
AD 2	74	White male	4,4
AD 3	82	White male	4,4
Mean AD age	76.7		
HtD 1	75	White male	2,3
HtD 2	58	White male	3,4
HtD 3	87	White male	3,3
Mean HtD age	73.3		

AMC, age-matched control; AD, Alzheimer's disease; HtD, heart disease.

Proteomic analysis by mass spectrometry

Aggregate proteins were separated by electrophoresis on SDS-polyacrylamide gels, and each lane was robotically sectioned into 12 segments of equal volume. Each segment was subjected to in-gel trypsin digestion as follows. Gel slices were destained in 50% methanol (Fisher), 50-mM ammonium bicarbonate (Sigma-Aldrich), followed by reduction in 10-mM Tris[2-carboxyethyl]phosphine (Pierce), and alkylation in 50-mM iodoacetamide (Sigma-Aldrich). Gel slices were then dehydrated in acetonitrile (Fisher), followed by the addition of 100-ng porcine sequencing-grade modified trypsin (Promega) in 50-mM ammonium bicarbonate (Sigma-Aldrich) and incubation at 37°C for 12–16 hours. Peptide products were then acidified in 0.1% formic acid (Pierce) and separated by reverse-phase chromatography on XSelect CSH C18 2.5-µm resin (Waters) on an in-line 150 × 0.075 mm column using the UltiMate 3000 RSLCnano system (Thermo). Peptides were eluted using a 45-min gradient from 98:2 to 65:35 buffer A:B ratio. Eluted peptides were ionized by electrospray (2.2 kV), followed by MS/MS analysis using higher-energy collisional dissociation (HCD) on an Orbitrap Fusion Tribrid mass spectrometer (Thermo) in top-speed data-dependent mode. MS data were acquired using the FTMS analyzer in profile mode at a resolution of 240,000 over a range from 375 to 1500 m/z. Following HCD activation, MS/MS data were acquired using the ion trap analyzer in centroid mode and normal mass range with precursor mass-dependent normalized collision energy between 28.0 and 31.0.

Proteins were identified by database search using Mascot (Matrix Science) with a parent ion tolerance of 3 ppm and a fragment ion tolerance of 0.5 Da. Scaffold (Proteome Software) was used to verify MS/MS-based peptide and protein identifications. Peptide identifications were accepted if they could be established with <1.0% false discovery by the Scaffold Local FDR algorithm. Protein identifications were accepted if they could be established with <1.0% false discovery and contained at least two identified peptides. Protein probabilities were assigned by the Protein Prophet algorithm[38].

Immunoprecipitation with 14-3-3 antibody and western-blot analysis

Tissues from AD, HtD, and AMC hippocampi, and cohorts of *C. elegans* 14-3-3 deletion worms, were flash-frozen and pulverized in a mortar and pestle cooled on dry ice as previously described[4]. Samples were incubated with DYNAL Protein-G magnetic beads coated with antibody against the human 14-3-3 conserved core region. Bound proteins were rinsed, eluted, and resuspended in 0.1-M HEPES buffer (pH 7.4) with 1% v/v sarcosyl, 5-mm EDTA, and protease inhibitors. After centrifugation for 30 min at 100,000 × g, pellets were resuspended as above, and immunoprecipitation (IP) complexes were resolved on 1% SDS-acrylamide gels. Aggregate complexes, isolated by 14-3-3 IP from ezetimibe-treated or control SH-SY5Y-APP_{Sw} neuroblastoma cells, were electrophoresed for 2 hours at 100 V on 4%–20% gradient Bis-Tris acrylamide gels (BioRad Life Science, Hercules, CA, USA) and transferred to nitrocellulose membranes (BioRad). Blots, blocked with bovine serum albumen (BSA, Pierce), were incubated for 14 hours at 4°C with primary antibodies to 14-3-3 (14-3-3 Pan-Antibody, 1:5000 dilution; ThermoFisher, Waltham, MA, USA) or to HK1 (MA5-14789; 1:10,000 dilution; ThermoFisher).

Structure retrieval and preparation

Structures of 14-3-3 paralogs (14-3-3S/σ, 14-3-3G/γ, 14-3-3Z/ζ) were obtained from Protein Database PDB (www.rcsb.org; accessed 25 May 2021) or modeled using I-TASSER (//zhanggroup.org/I-TASSER/; accessed 2 June 2021). Retrieved and modeled structures were prepared by adding polar hydrogens and missing atoms/side chains, as determined by Schrödinger Maestro (version 11.9.011).

PPI modeling

PPIs were modeled using Hex (v.8.0), an interactive PPI modeling and molecular-superposition program that predicts the most stable (lowest $\Delta G_{binding}$) interaction of target proteins. PPI complexes modeled under default parameters were analyzed to detect druggable pockets or interfaces using the Discovery Studio Receptor Cavities plug-in[12].

Molecular-dynamic simulations

Target PPIs alone, or in complexes with drugs, were simulated using Desmond. Complexes were prepared using Maestro preprocessing wizard with default parameters, immersed in orthorhombic boxes, and neutralized by adding the requisite ions (Na^+, Cl^-); a further 0.15-M NaCl was added to mimic physiological conditions. Temperature and pressure were held constant at 300°K and 1.1023 bar, respectively. Each simulation was initiated with a random seed number, maintained for 200 ns (unless otherwise indicated), and replicated ≥3 times with new seeds. Simulation trajectories were analyzed using Maestro Viewer's Simulation Interaction Diagram plugin.

High-throughput virtual screening

An FDA-approved drug library was retrieved from SelleckChem and converted to SYBYL TRIPOS format using Discovery Studio Visualizer. The top 10% of drugs from first-stage virtual docking screens (AutoDock-Vina) were reanalyzed with AutoDock-Vina in

high-precision mode, followed by MM-GBSA simulations to assess $\Delta G_{binding}$ for each drug::target complex.

Statistical analysis

The significance of differences between groups was assessed by homoscedastic "Student's" t tests for groups of $N \geq 8$ with like variance; smaller groups, or groups of unequal variance, used heteroscedastic t tests (Excel option 3). The intra-experiment significance of proportion shifts was assessed by chi-squared or Fisher's exact tests (as appropriate to group sizes). As indicated in figure legends, multiple replicate assays were sometimes treated as single points, and inter-experimental reproducibility was assessed by heteroscedastic t tests.

Results

Protein aggregation is significantly increased in the hippocampi of HtD and AD individuals

We showed that hippocampal aggregates are at least 60% more abundant in postmortem brains from AD than from AMCs[4]. Subsequent studies of brain aggregates from HtD patients revealed surprisingly similar increments. Figure 1A shows examples of sarcosyl-insoluble aggregate proteins resuspended in Laemmli buffer at 100°C, resolved by acrylamide-gel electrophoresis, and stained for protein. Quantitations of protein per lane, summarized in Figure 1B, indicate a 65% increase in HtD aggregates relative to AMCs and an ~80% increase in aggregates from AD patients carrying the *APOE(ϵ4,ϵ4)* genotype (each $P < 0.04$ by heteroscedastic t test). The high aggregate burden in "AD44" patients is attributed to the combination of AD and the *APOE4,4* genotype[4].

14-3-3G and HK1 are enriched in HtD and AD brain aggregates

We predicted 14-3-3 proteins to be very influential in AD-specific aggregation using neural networks, as we had previously reported[12,39,40]. Since all seven human 14-3-3 paralogs are enriched in AD aggregates[4,12], detergent-insoluble aggregates were isolated by pulldown with antibody to the 14-3-3 central core, conserved across the 14-3-3 family. The aggregate content of 14-3-3G (gamma) protein is elevated approximately twofold in AD and nearly threefold in HtD hippocampi (each $P < 0.0001$) over AMC (Fig. 1C). HK1, a PPI partner of 14-3-3G, was not observed in

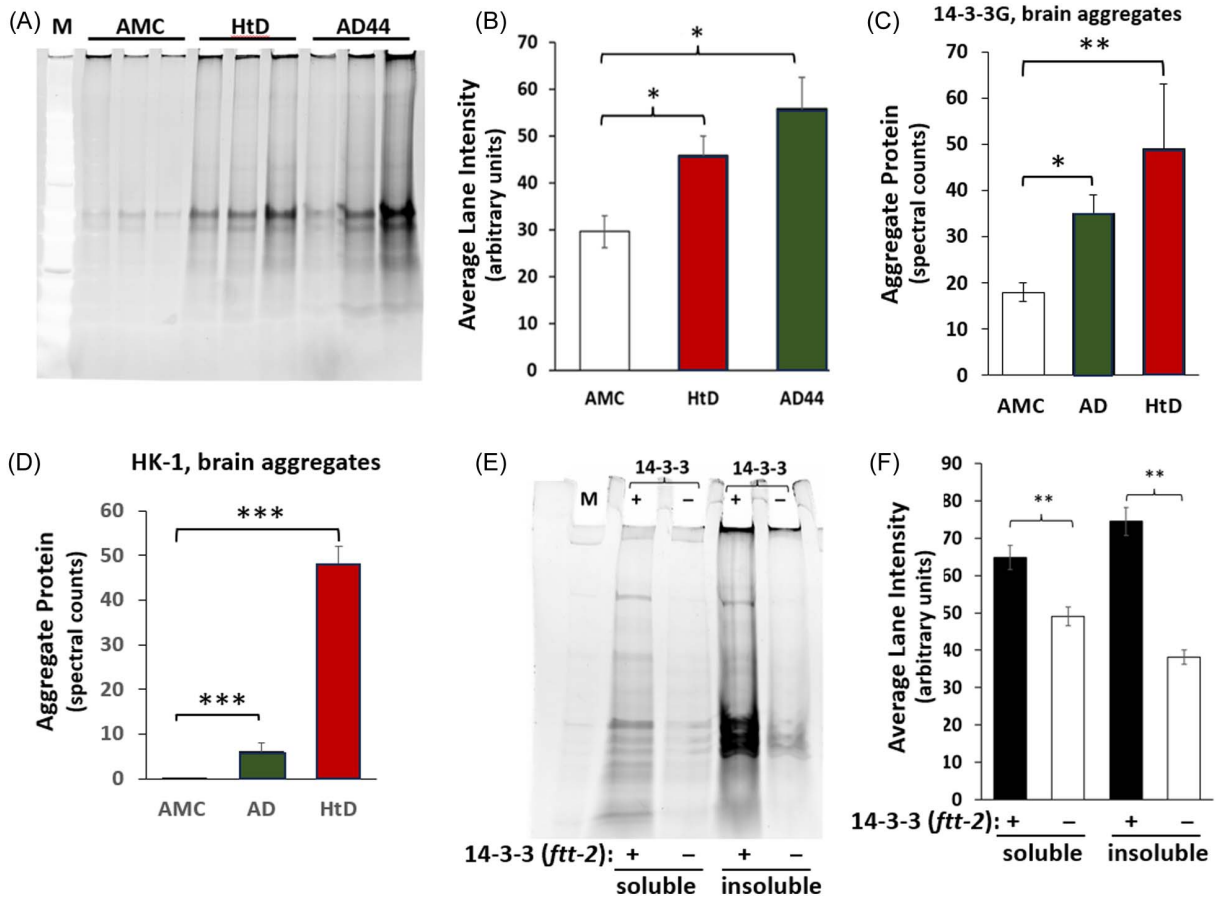

Figure 1. Analysis of sarcosyl-insoluble aggregates reveals significantly elevated 14-3-3 and associated proteins in heart-disease (HtD) tissue aggregates. (A) Gel electrophoresis of resuspended hippocampal aggregate proteins from age-matched controls (AMCs), HtD, and Alzheimer's patients carrying the *APOE4/E4* genotype (AD44). **(B)** Quantitation of gel lanes, as illustrated in panel A ($N = 5–6$ per group). *Adjusted $P < 0.04$ by heteroscedastic t test, treating each experiment as a single data point. Enrichment of **(C)** 14-3-3G and **(D)** hexokinase-1 (HK1) in aggregates from AD or HtD hippocampi, based on LC-MS/MS spectral counts identified as peptides from these proteins. **(A,C,D)** Significances of intergroup differences were determined by chi-squared or Fisher exact tests, as appropriate to the observed numbers: *$P < 0.05$; **$P < 0.01$; ***$P < 0.001$. **(E)** Detergent-soluble and detergent-insoluble aggregates are reduced in *C. elegans* with a 14-3-3 knockout (*ftt-2* KO, "–") versus WT ("+"). **(F)** Quantitation of soluble and insoluble aggregates from *C. elegans ftt-2* knockout strain versus WT (biological $N = 5–6$ per group). **$P < 0.01$ by heteroscedastic t test, treating each experiment as a single data point to evaluate reproducibility.

AMC aggregates but was consistently found in AD hippocampal aggregates and elevated a further tenfold in HtD aggregates (each $P < 0.0001$), as shown in Figure 1D.

Deletion of a 14-3-3 gene in *C. elegans* reduces soluble and insoluble aggregates

The enrichment of 14-3-3 proteins in HtD and AD aggregates led us to ask whether genetic deletion of one of two *C. elegans* 14-3-3 genes, *ftt-2*, would reduce protein aggregation. Both sarcosyl-soluble and sarcosyl-insoluble aggregates were isolated from a *C. elegans* 14-3-3/*ftt-2* knockout strain. Soluble protein aggregates were reduced by 35% and insoluble aggregates by ~50% (each $P < 0.01$) in day-3 adults relative to an isogenic wild-type control strain (Bristol-N2 [DRM]) (Fig. 1E,F).

Machine-learning analyses of AD interactomes identify aggregate "lynchpin" PPIs

Interactome modeling based on aggregate-cross-link analysis identified numerous PPIs unique to AD[41]. To identify influential interactions that may play key roles in initiating, augmenting, and stabilizing AD β-amyloid aggregates, we calculated the fold increase in the number of direct contacts (i.e., degree) of each node in the AD interactome as its AD/AMC "degree ratio" (Fig. 2A). The 14-3-3G subnetwork comprises 18 interacting partners that were absent from AMC aggregates but observed at 50–340 spectral counts per sample in AD and thus are effectively disease-specific. Another four partners were less abundant in AD aggregates, and two did not change significantly. We focused on the HK1 interaction with 14-3-3G based on their previous implication in AD and HtD[20,22,24,25,31,42].

Screening FDA-approved drugs *in silico*

We used our own in-house implementation of molecular-modeling tools to create a 3D model of the adherent protein pair, 14-3-3G:: HK1 (Fig. 2B). Molecular-dynamic simulations of this PPI predict stable interaction in the absence of drug. The 14-3-3G::HK1 model then served as a target for computational multi-stage screening of structures among the >1800 FDA-approved drugs (i.e., all available drugs except chemotherapy agents, excluded due to genotoxicity) for predicted affinity to this protein-interface target. Estimates of the binding free energy prioritized six top drugs, ranked by predicted affinity for the 14-3-3G:: HK1 interface (Table 1). The top-ranked candidates were pursued by literature and patent research and *in silico* prediction of ADMET properties (e.g., computational predictions of solubility, mouse and human pharmacokinetics, and extent of blood-brain-barrier penetration) using Discovery Studio™. Six drugs were initially predicted to have robust binding to this target; ezetimibe was selected for validation and pursuit as a candidate aggregation inhibitor, targeting disruption of 14-3-3G::HK1 adhesion. The free energy of ezetimibe binding ($\Delta G_{binding}$) at the 14-3-3G::HK1 interface is −9.7 kCal/mol (Fig. 2C). Intermolecular hydrogen bonds between 14-3-3G and HK1 were predicted across a 200-ns molecular-dynamic simulation, in the absence versus presence of ezetimibe (Fig. 2D), excluding the first 10 ns to permit initial equilibration. Ezetimibe was estimated to reduce H bonds between the target proteins by ~30% ($P < 1E{-}142$ by two-tailed t test).

Ezetimibe blocks 14-3-3G interaction with HK1

To test the proposed mechanism of drug action, we asked whether ezetimibe impedes 14-3-3G interaction with HK1 in

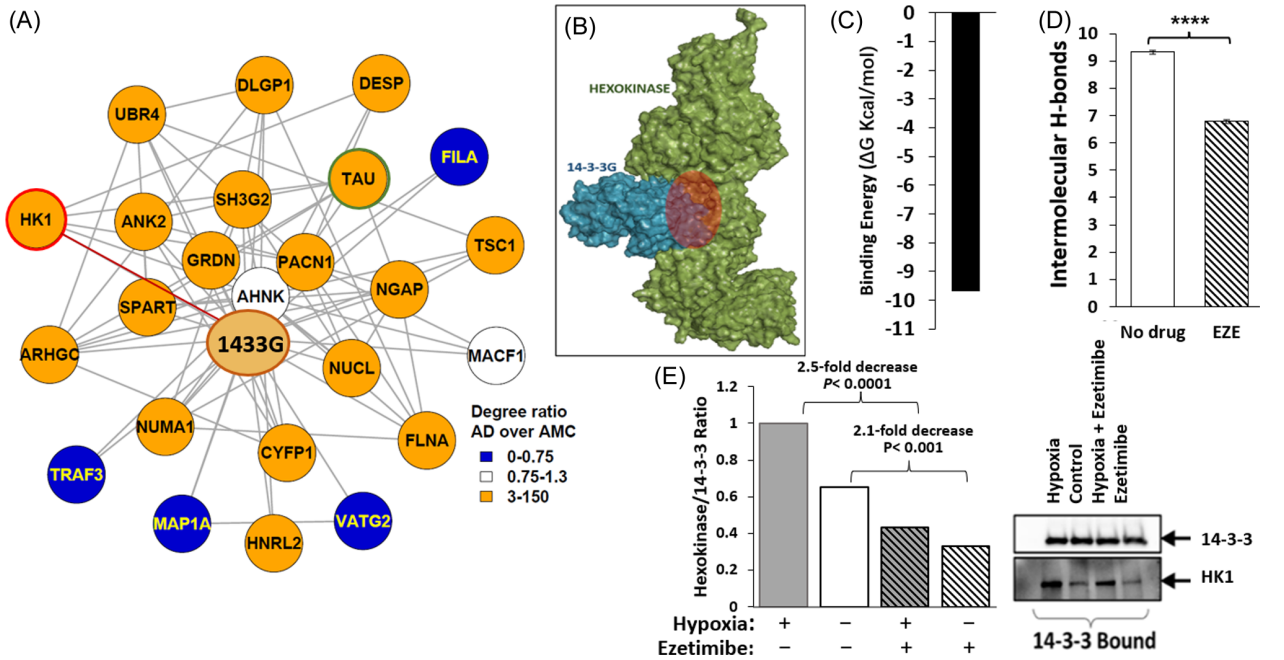

Figure 2. 14-3-3 proteins co-aggregate with HK1 in AD and HtD brain tissue. (A) Interactome subnetwork of 14-3-3G and its direct contacts, derived by cross-linking Aβ-IP aggregates from AMC versus AD hippocampi. **(B)** Molecular model of 14-3-3G (blue) adhesion to HK1 (green). The cross-link-based interface, coinciding with the druggable pocket targeted in library screens, is highlighted in maroon. **(C)** The FDA-approved drug ezetimibe is predicted to bind avidly to the 14-3-3G::HK1 interface, based on ΔG values from molecular-dynamic simulations. **(D)** Average intermolecular H bonds between 14-3-3 and HK1 were predicted for the span from 10–200 ns of simulation; error bars represent ± SEM. ****$P < 1E{-}142$ by two-tailed t test. **(E)** Co-immunoprecipitation of 14-3-3 recovers less hexokinase (indicated by lower HK1/14-3-3 ratios) from human SY5Y-APP_{Sw} neuroblastoma cells treated for 48 hours with 10-μM ezetimibe. The histogram combines data from triplicate assays (each $P < 0.01$ by two-tailed heteroscedastic t tests). Within-assay P values (indicated over brackets) were assessed by chi-squared tests.

Table 1. Top drugs predicted to bind the 14-3-3G::hexokinase-1 interface.

Drug Name	Binding Affinity	Drug Type (Condition Treated)	Aggregate Reduction (%)	Chemotaxis Rescue (%)	Side Effects, Other Demerits
Conivaptan	–11.4	Vasopressin inhib. (low blood sodium)	48.6	53.6	Hypotension
Lumacaftor	–10.6	Protein chaperone (cystic fibrosis)	66.7	48.5	Hepatotoxicity
Ebastine	–10.2	H_1 antihistamine; low narcolepsy	8.3	15.5	No blood-brain-barrier transit
Digitoxin	–10.1	Cardiac glycoside (congestive heart failure)	7.2	52.8	Toxicity, other side effects
Astemizole	–10	Antihistamine used to treat allergies	16.6	11.8	May cause arrhythmia
Ezetimibe	–9.7	Lowers blood cholesterol (hyperlipidemia)	55	52.3	Diarrhea, respiratory infections (rare)

aggregates from human cells. SH-SY5Y-APP_{Sw} neuroblastoma cells, expressing a mutant amyloid precursor protein (APP_{Sw}) implicated in familial AD, were treated with ezetimibe under normal conditions or after a hypoxic interval to simulate the effects of myocardial infarction[5]. Complexes containing 14-3-3 were recovered from cell lysates by immunoprecipitation, and proteins were separated on electrophoresis on SDS-polyacrylamide gels, immobilized on nitrocellulose membranes, and western blots were then probed with antibodies to 14-3-3 or HK1. Ezetimibe blocked 14-3-3::HK1 interaction, so that 14-3-3 IP yielded only ~40% as much bound HK1 relative to 14-3-3 recovery (e.g., "14-3-3 bound" in Fig. 2E) from hypoxic cells in three independent cultures. Nonhypoxic cells had only 65% as much HK1 co-IP recovery as hypoxic cells, of which ezetimibe blocked about half (Fig. 2E).

Cultured human cells are protected by ezetimibe from amyloid aggregate accrual

We next evaluated ezetimibe for protection of human cell lines that model AD-like aggregation. Neuroblastoma cell lines (SY5Y-APP_{Sw} and SY5Y-tau) and embryonic kidney cells (HEK-tau) were treated with ezetimibe at several concentrations and then stained with Thioflavin T or Proteostat to quantify relative amyloid burden. SY5Y-APP_{Sw} cells treated with 0.1-μM ezetimibe had only ~40% as much aggregate as control cells exposed to vehicle without drug. HEK-tau and SY5Y-tau cells exposed to 0.01-μM ezetimibe had ~60% and 32% as much aggregate staining, respectively, as control cells (Fig. 3A–C summarizes data and shows typical images at optimal drug concentrations).

Ezetimibe enhances autophagy, reducing protein aggregate levels

Autophagy plays a key role in the clearance of aggregates and damaged organelles[43,44]. Defective autophagy has been repeatedly implicated as a mechanistic contributor to the development and progression of neurodegenerative disorders, consistent with the failure to clear toxic protein aggregates from cells in which autophagy is deficient[43,44]. 14-3-3 proteins modulate autophagy by binding to regulatory proteins such as Beclin-1[45]. Given the evidence that aggregation in human-brain-derived cells is alleviated by ezetimibe (Fig. 3A–C) and that this drug disrupts 14-3-3G::HK1 interaction (Fig. 2E), we assessed its impact on autophagy. Ezetimibe at 0.1 μM significantly enhanced autophagy in SY5Y-APP_{Sw} neuroblastoma cells (Fig. 3D; $P < 0.02$). In view of our earlier evidence that this same cell line accrues 60% less aggregate in the presence of ezetimibe (Fig. 3A), this result suggests that ezetimibe either activates autophagy (perhaps by liberating 14-3-3G, which stimulates autophagy, from aggregates) or reduces the demand for it by lowering the aggregate burden. Physiological levels of 14-3-3 were shown to be depleted in AD[22], thereby diminishing autophagy by disruption of 14-3-3 interactions[45].

Ezetimibe reduces aggregation in cultured neuronal and glial cells under hypoxia

Since 14-3-3G and HK1 are enriched in brain aggregates from AD and especially HtD (Fig. 1C,D), we evaluated the aggregation-limiting effects of ezetimibe in cultured human neuronal and glial cells. NT2 (neuroblastoma) and T98G (glioma) cell lines were exposed to ezetimibe at 0.01–1 μM for 48 hours, either with or without prior hypoxia (94% N_2, 6% CO_2 for 7 hours), and aggregates were then stained with Thioflavin T. While hypoxia alone increased aggregation by 18%–40%, ezetimibe conferred significant protection against protein aggregation to both neuronal and glial cells, with or without hypoxia (Fig. 4A and 4B, respectively).

Ezetimibe protects nematodes from amyloid aggregate accrual

C. elegans strain CL2355 is a model of amyloid aggregation due to neuronal expression of human $A\beta_{1-42}$, resulting in impaired chemotaxis, either with age[4] or following late-larval induction[46]. While chemotaxis (attraction to n-butanol) is >90% in young wild-type worms, it drops to 37% in aged controls; however, exposure to 10-μM ezetimibe restores it to 72% (Fig. 4C; $P < 0.0001$). Strain VH255, a model of AD in which normal human tau is highly expressed in body-wall muscle, undergoes progressive paralysis with age. Continuous ezetimibe exposure from egg hatch reduced paralysis by 40% on day 8 and 50% on day 13 post-hatch (Fig. 4D).

Ezetimibe reduces aggregates in *C. elegans* expressing neuronal $A\beta_{1-42}$:: *mCherry*

C. elegans strain UA355 combines transgenes encoding human $A\beta_{1-42}$ fused in-frame to *mCherry* and human ApoE4, co-expressed in glutamatergic neurons. These worms accrue red-fluorescent Aβ amyloid in the neurons of mature adults, largely rescued by ezetimibe. UA355 worms were treated from egg hatch for 5 days with 10-μM ezetimibe or vehicle and then assessed for Aβ::mCherry amyloid deposits, quantified in fluorescence images (see images and histogram, Fig. 4E). Ezetimibe reduced $A\beta_{42}$::mCherry accrual >60% in these worms (two-tailed

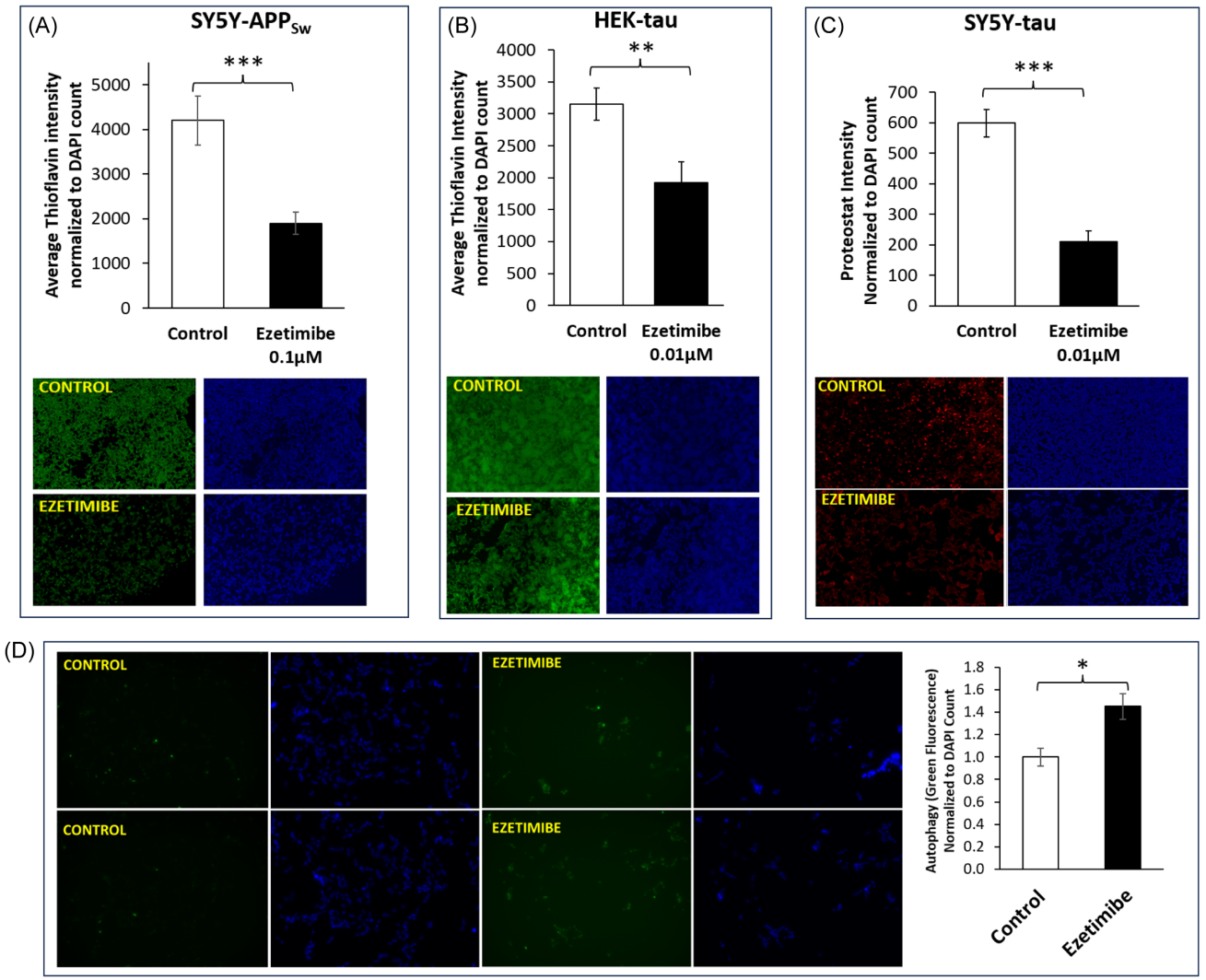

Figure 3. Ezetimibe reduces aggregation in three human-cell models of AD aggregation. (A) SY5Y-APP_{Sw} neuroblastoma cells expressing an APP_{Sw} transgene from a familial-AD pedigree; **(B)** HEK-tau cells, human embryonic kidney cells expressing normal human tau; and **(C)** SY5Y-tau, human neuroblastoma cells expressing normal human tau. Cells were imaged after 48 hours. of treatment with vehicle (control) or ezetimibe at the near-optimal doses indicated. $^{**}P < 0.01$; $^{***}P < 1E{-}5$, by two-tailed t tests (each $N \geq 30$). In the typical images under panels **(A)–(C)**, green fluorescence reflects Thioflavin T staining for amyloid; blue fluorescence shows DAPI staining of nuclear DNA, used to count cells per field. Under panel **(C)**, SY5Y-tau cells were treated with ezetimibe and stained with Proteostat, another molecular-rotor dye, showing a reduction in tau aggregation after ezetimibe. **(D)** Images of SY5Y-APP_{Sw} cells treated with rapamycin (10 μM for 24 hours) to induce autophagy, ± ezetimibe as indicated. The histogram summarizes green fluorescence intensity per cell (directly proportional to autophagy induction), calculated from fluorescence images; error bars represent SEM. $^{*}P < 0.02$, based on a two-tailed heteroscedastic t test for three independent experiments assaying different cell expansions.

t test $P < 0.01$) and reduced age-associated neuron loss 10%–20% in a *C. elegans* neuronal-reporter strain (Fig. 5; $P < 0.03$).

Ezetimibe significantly reduces the incidence of AD and related dementias (ADRD) in normal elderly subjects and in a high-risk subset of patients with CAD

We analyzed data in the PharMetrics-Plus IQVIA database, comprising 2006–2020 clinical data. From this database, we found 4361 patients receiving ezetimibe and selected ~945,000 AMCs (mean age 65 ± 5 y). Untreated and treated groups have comparable sex ratios (46% vs. 54% males), and prevalence of hypertension (37% vs. 33%) and diabetes (18% vs. 17%). Remarkably, the incidence of ADRD during follow-up differed by eightfold (0.8% vs. 0.1%), reflecting a relative risk (RR) of 0.14 for those on ezetimibe (Table 2; 95% confidence interval 0.06–0.34; $P < 0.0001$), using a time-dependent regression model to adjust for the observation time interval.

A subset of these subjects had been diagnosed with CAD. Among those with CAD, we identified 547 patients prescribed ezetimibe and 73,387 CAD/CHD AMCs. In this cohort, with a known elevated likelihood of subsequent AD or related cognitive impairment, the RR for ADRD diagnosis during follow-up was 0.122 for ezetimibe recipients relative to controls (Table 3; 95% C.I.: 0.02–0.88; $P < 0.006$). Taken together, these findings suggest that ezetimibe confers highly significant protection from ADRD to individuals with and without CAD. While the mechanisms warrant further investigation, these data provide compelling evidence to support the pursuit of ezetimibe for neuroprotection, especially in those at elevated risk of ADRD.

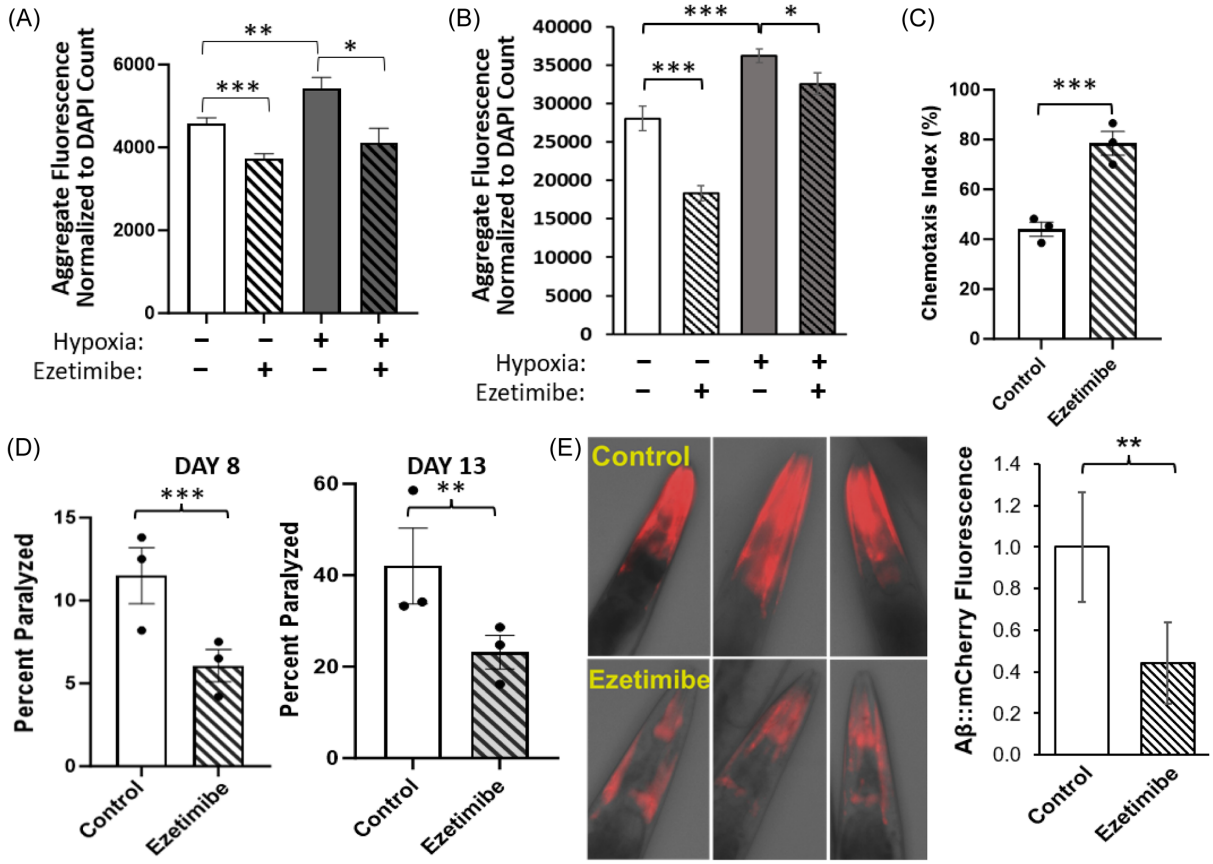

Figure 4. Ezetimibe reduces aggregation and its sequelae in multiple AD models. Ezetimibe reduces protein aggregation in **(A)** human NT2 neuroblastoma cells and **(B)** human T98G glioma cells. **(C)** Ezetimibe treatment of *C. elegans* strain CL2355, expressing human $A\beta_{1-42}$ in all neurons, improves chemotaxis greater than twofold. **(D)** Ezetimibe treatment of *C. elegans* strain VH255, expressing normal human tau protein in muscle, reduces paralysis at days 8 and 13 post-hatch. **(E)** Ezetimibe (10 μM) reduces amyloid burden in transgenic *C. elegans* strain expressing Aβ::mCherry in neurons (red fluorescence). **(A,B)** Significance of differences by two-tailed t tests (each $N > 30$): *$P < 0.05$; **$P < 0.005$; ***$P < 0.001$; **(C–E)** *$P < 0.05$; **$P < 0.01$; ***$P < 1E{-}4$ by two-tailed heteroscedastic t tests.

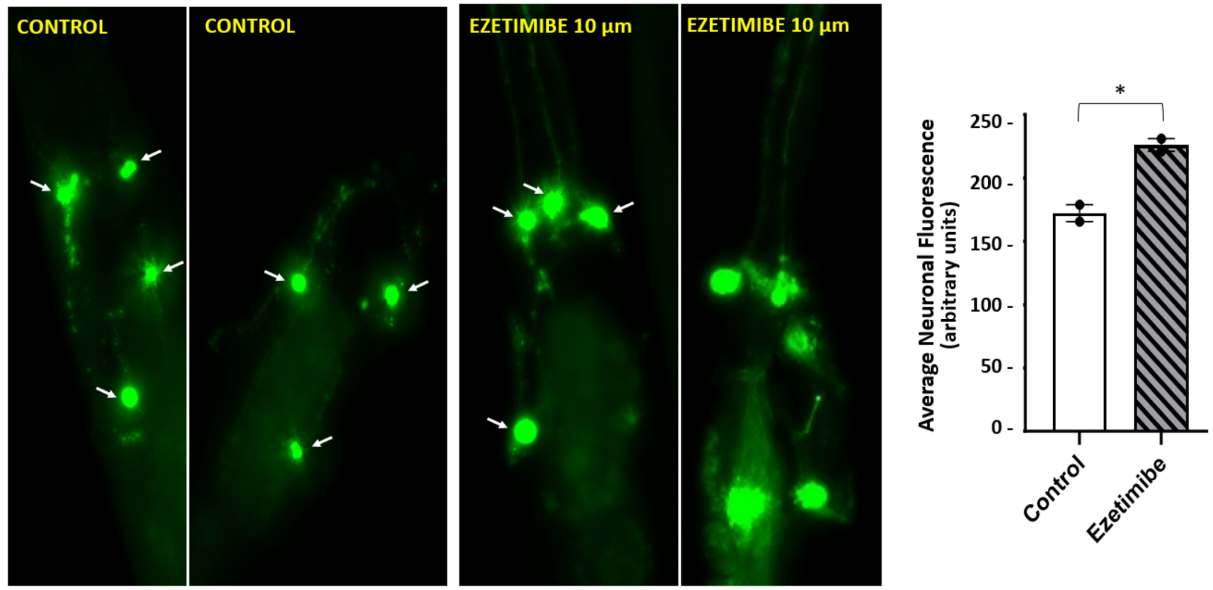

Figure 5. Ezetimibe protects against age-associated neuronal loss. Worms of *C. elegans* strain UA57, expressing GFP in all dopaminergic neurons, were treated with 0.01% DMSO (control) or 10-μM ezetimibe and imaged at 22 days post-hatch, capturing fluorescence with a Keyence microscope BZ-X series (IL, USA). The histogram shows replicate results and means ± 1 standard deviation. *The intergroup difference is significant by a two-tailed heteroscedastic t test at $P < 0.03$.

Table 2. General characteristics of populations used to calculate relative risk ± ezetimibe.

Characteristics	Study Population (n, %)		SMD
	No Ezetimibe Use	Ezetimibe Use	
Total number (n, %)	944,983 (100.0)	4,361 (100.0)	0.017
Entry age (mean [SD])	64.94 (5.20)	64.86 (4.58)	0.156
Sex = M (%)	437,410 (46.3)	2,357 (54.0)	0.014
Follow-up duration category (% of subjects)			
<1 y	247,726 (26.2)	1,119 (25.7)	
1–3 y	29609.2 (31.3)	1,387 (31.8)	
>3 y	401,165 (42.5)	1,855 (42.5)	
Stroke	11,521 (1.2)	31 (0.7)	0.052
Hypertension	352,882 (37.3)	1,427 (32.7)	0.097
Diabetes	169,247 (17.9)	736 (16.9)	0.027
Depression	41,626 (4.4)	97 (2.2)	0.122
CKD	51,126 (5.4)	145 (3.3)	0.102
CAD	73,387 (7.8)	547 (12.5)	0.159
AMI	1,628 (0.2)	7 (0.2)	0.003
ADRD	7,467 (0.8)	5 (0.1)	0.101

SMD, standardized mean difference; CKD, chronic kidney disease; CAD, coronary artery disease; AMI, acute myocardial infarction; ADRD Alzheimer's disease and related dementias.
Relative risk = 0.14 (95% confidence interval 0.06–0.34, P < 0.0001).

Table 3. Analysis of characteristics and Alzheimer's disease and related dementias (ADRD) incidence among coronary artery disease (CAD) patients, used to calculate the relative risk in this ADRD-predisposed subgroup, ± ezetimibe.

Characteristics	Study Population (n, %)		SMD
	No Ezetimibe Use	Ezetimibe Use	
Total number (n, %)	73,387 (100.0)	547 (1000)	0.148
Entry age (mean [SD])	66.56 (4.89)	65.85 (4.61)	0.217
Sex = M (%)	51,342 (70.0)	434 (79.3)	0.104
Follow-up duration category (% of subjects)			
<1 y	6,861 (9.3)	68 (12.4)	
1–3 y	18,481 (25.2)	140 (25.6)	
>3 y	48,045 (65.5)	339 (62.0)	
Stroke	2152 (2.9)	9 (1.6)	0.086
Hypertension	49,222 (67.1)	297 (54.3)	0.264
Diabetes	22,068 (30.1)	92 (168)	0.317
Depression	3,467 (4.7)	11 (2.0)	0.151
CKD	7,888 (107)	21 (3.8)	0.268
CAD	73,387 (100.0)	547 (100.0)	<0.001
AMI	1,608 (2.2)	7 (1.3)	0.07
ADRD	1,076 (1.5)	1 (0.2)	0.142

SMD, standardized mean difference; CKD, chronic kidney disease; CAD, coronary artery disease; AMI, acute myocardial infarction; ADRD Alzheimer's disease and related dementias.
Relative risk = 0.122 (95% confidence interval 0.02–0.88, P < 0.006).

Discussion

The worldwide incidence of dementia is projected to increase from 57.4 million cases in 2019 to over 150 million by 2050, mainly due to the aging of the population[47]. AD and ADRD pose a daunting challenge to those afflicted, their caregivers, and the health-care system undertaking their treatment. Those with predisposing conditions, which include advanced age, hypertension, HtD, obesity, diabetes, traumatic brain injury, or the presence of an *APOE4* allele, may be prime candidates for prophylactic "off-label" treatment with ezetimibe.

The mechanism through which HtD elevates ADRD risk has been the subject of intensive investigation. Cardiac aging and AMI can increase reactive oxygen species, implicated in the

etiology of chronic inflammation and ADRD[48]. Inflammatory serum markers are elevated in AD[49], and neuroinflammation is a common sequela of AMI[50–52]. These features suggest early roles for inflammation in both AMI and AD. Age-associated chronic inflammation, even of moderate severity, contributes to protein aggregation in and around neurons[53], which in turn augments neuroinflammation[54], creating a positive-feedback loop or vicious cycle. Both aggregation and inflammation have been implicated in the onset and progression of neurodegenerative disorders and in the underlying process of aging[55,56].

All paralogs of the 14-3-3 protein family share a conserved central domain comprising nine helical segments and divergent N- and C-terminal domains that are intrinsically disordered[12]. Through these unstructured domains, in concert with the central "cradle," 14-3-3 proteins form induced-fit interactions with diverse partners to regulate diverse signaling pathways, including autophagy, cellular metabolism, and stress responses, with impacts on neurodegeneration. We reported that 14-3-3 paralogs are enriched in aggregates from the brain, muscle, and heart[4,6,10,57]. Detection of 14-3-3 proteins in cerebrospinal fluid is diagnostic of Creutzfeldt-Jakob disease but may also be associated with other dementias, including Alzheimer's, or intracerebral hemorrhages[58]. Immunostaining of AD-patient hippocampi for tau suggests colocalization of 14-3-3 proteins with neurofibrillary tangles[42]. Individuals with specific polymorphisms in both tau and 14-3-3Z are at a 2.5-fold lower risk of AD[59]. Interacting partners of 14-3-3 proteins, such as FOXO and TFEB transcription factors, coordinate physiological processes governing lifespan, stress responses, and autophagy, whereas other partners, including the p53 tumor suppressor, p21/WAF1, and the p85 regulatory subunit of class-I PI3K, modulate cell proliferation, replicative senescence, cancer, insulin and insulinlike signaling, and longevity[20,60,61]. We found that 14-3-3 proteins themselves, as well as their immediate interacting contacts, are enriched in hippocampal aggregates in AD and HtD patients[12,57].

RNAi knockdown of either 14-3-3 proteins or one of their critical disease-specific interacting partners reduces aggregate burden[12]. This strategy would not be advisable to alleviate the risk of future diseases in light of the evidence that disruption of 14-3-3 proteins may cause or exacerbate diabetic cardiomyopathy[62] and neurodegeneration[20,63–66]. We therefore opted not to target the interactive terminal regions of these proteins but rather to disrupt an interface unique to pathological aggregates—the 14-3-3G::HK1 adhesion zone. This PPI is abundant in AD aggregates but absent from healthy brains of the same age, implying that it is disease-specific but not symptomatic of aging per se.

The neuroprotective effects of ezetimibe were not unheralded, as it had been previously shown to improve memory in mice fed a high-fat diet[67], but no mechanism had been proposed. Ezetimibe was also shown to reduce neuronal apoptosis by activating autophagy in a rat model of arterial occlusion[68]. While these benefits may have been assumed to be secondary to cholesterol reduction via sparing of vascular inflammation, our human-cell-culture and intact-nematode experiments support a direct neuroprotective effect via disruption of aggregate-specific protein interactions.

Enhanced autophagy offers an alternative mechanism, given the prior evidence that 14-3-3G itself promotes autophagy[45]; its sequestration in aggregates would thus be expected to impair that process. Ezetimibe reduction of aggregates in both *C. elegans* and human-cell-culture models of AD could be attributed to its ability to enhance autophagy (**Fig. 3D**), an expected consequence of 14-3-3G sequestration. However, in view of the vicious cycle between inflammation and aggregation, an anti-inflammatory mechanism (possibly secondary to rescue from aggregation) cannot be excluded.

The animal and cultured-cell models for which we present data substantiate that ezetimibe indeed reduces aggregates across a broad spectrum of biological systems and that it does so by blocking or dissociating dysfunctional (or nonfunctional) interaction between 14-3-3G and HK1. However, the most compelling evidence that ezetimibe can prospectively *prevent AD* comes from our interrogation of a large clinical database. We employed a time-dependent regression model to evaluate the association between ezetimibe use and ADRD incidence in a large compilation of clinical data collected over varying observation intervals. Although this was a retrospective analysis of previously collected data, the magnitude of the ezetimibe effect (greater than sevenfold reduction in risk, $P << 10^{-4}$ for the general aged population; eightfold, $P < 0.006$, for the CAD subset) far exceeds the protection arising from any previous intervention. Further studies are needed to optimize doses for repurposing this drug to protect those at the highest risk of ADRD. As only minor side effects of ezetimibe were identified during widespread use for over 20 y, we believe that the potential neuroprotective benefits far outweigh the risks.

Acknowledgments

We thank Drs. Guy and Kim Caldwell for providing *C. elegans* strain AU355 expressing ApoE4 and Aβ::mCherry, and Dr. Sue T. Griffin for providing human hippocampal tissue from the UAMS Brain Bank for our study.

Funding

This work was supported by funding from the following grants: Grant 1R01 AG062254 to S.A. and R.J.S.R. from the National Institute on Aging (NIA/NIH); Merit Review Award I01 BX001655 and Senior Research Career Scientist Award IK6 BX004851 to R.J.S.R. from the U.S. Department of Veteran Affairs; and an award to M.B. from the Inglewood Scholars Program.

Author Contributions

S.A., R.J.S.R., and S.V. designed and conceptualized this study. S.A., A.G., N.M., M.B., R.A., S.P., and J.J.A. developed and executed methodology. R.J.S.R. and S.A. obtained funding support and provided supervision to other investigators. S.A., A.G., R.J.S.R., M.B., C.N., and S.V. wrote the initial draft of this article, and S.A., A.G., and R.J.S.R. edited and revised this article.

Conflicts of Interests

The authors have filed a patent application (currently pending) for repurposing ezetimibe to reduce the likelihood of cognitive decline in at-risk individuals. They declare no other conflicts of interest.

Data Sharing

All relevant data will be promptly shared upon request.

References

1. Nandi A., Counts N., Broker J., Malik S., Chen S., Han R., … Bloom D.E. (2024). Cost of care for Alzheimer's disease and related dementias in the United States: 2016 to 2060. *N. P. J. Aging* **10**(1), 13. PMID: 38331952; doi: 10.1038/s41514-024-00136-6.
2. Jaisa-Aad M., Munoz-Castro C., & Serrano-Pozo A. (2024). Update on modifiable risk factors for Alzheimer's disease and related dementias. *Curr. Opin. Neurol.* **37**(2), 166–181. PMID: 38265228; doi: 10.1097/WCO.0000000000001243.
3. Ostergaard S.D., Mukherjee S., Sharp S.J., Proitsi P., Lotta L.A., Day F., … Scott R.A. (2015). Associations between potentially modifiable risk factors and Alzheimer disease: A Mendelian randomization study. *PLoS Med.* **12**(6), e1001841. PMID: 26079503; doi: 10.1371/journal.pmed.1001841.
4. Ayyadevara S., Balasubramaniam M., Parcon P.A., Barger S.W., Griffin W.S., Alla R., … Shmookler Reis R.J. (2016). Proteins that mediate protein aggregation and cytotoxicity distinguish Alzheimer's hippocampus from normal controls. *Aging Cell* **15**(5), 924–939. PMID: 27448508; doi: 10.1111/acel.12501.
5. Mainali N., Li X., Wang X., Balasubramaniam M., Ganne A., Kore R., … Ayyadevara S. (2023). Myocardial infarction elevates endoplasmic reticulum stress and protein aggregation in heart as well as brain. *Mol. Cell Biochem.* PMID: 37922111; doi: 10.1007/s11010-023-04856-3.
6. Ayyadevara S., Mercanti F., Wang X., Mackintosh S.G., Tackett A.J., Prayaga S.V., … Mehta J.L. (2016). Age- and hypertension-associated protein aggregates in mouse heart have similar proteomic profiles. *Hypertension* **67**(5), 1006–1013. PMID: 26975704; doi: 10.1161/HYPERTENSIONAHA.115.06849.
7. Blennow K., Hardy J., & Zetterberg H. (2012). The neuropathology and neurobiology of traumatic brain injury. *Neuron* **76**(5), 886–899. PMID: 23217738; doi: 10.1016/j.neuron.2012.11.021.
8. Ayyadevara S., Ganne A., Hendrix R.D., Balasubramaniam M., Shmookler Reis R.J., & Barger S.W. (2019). Functional assessments through novel proteomics approaches: Application to insulin/IGF signaling in neurodegenerative disease'. *J. Neurosci. Methods* **319**, 40–46. PMID: 30412730; doi: 10.1016/j.jneumeth.2018.11.005.
9. Ayyadevara S., Balasubramaniam M., Gao Y., Yu L.R., Alla R., & Shmookler Reis R. (2015). Proteins in aggregates functionally impact multiple neurodegenerative disease models by forming proteasome-blocking complexes. *Aging Cell* **14**(1), 35–48. PMID: 25510159; doi: 10.1111/acel.12296.
10. Ayyadevara S., Balasubramaniam M., Suri P., Mackintosh S.G., Tackett A.J., Sullivan D.H., … Dennis R.A. (2016). Proteins that accumulate with age in human skeletal-muscle aggregates contribute to declines in muscle mass and function in Caenorhabditis elegans. *Aging (Albany NY)* **8**(12), 3486–3497. PMID: 27992858; doi: 10.18632/aging.101141.
11. Dillin A., & Cohen E. (2011). Ageing and protein aggregation-mediated disorders: From invertebrates to mammals. *Philos. Trans. R. Soc. Lond. B Biol. Sci.* **366**(1561), 94–98. PMID: 21115535; doi: 10.1098/rstb.2010.0271.
12. Ganne A., Balasubramaniam M., Mainali N., Atluri P., Shmookler Reis R.J., & Ayyadevara S. (2022). Physiological consequences of targeting 14-3-3 and its interacting partners in neurodegenerative diseases. *Int. J. Mol. Sci.* **23**(24). PMID: 36555098; doi: 10.3390/ijms232415457.
13. Cuanalo-Contreras K., Park K.W., Mukherjee A., Millan-Perez Pena L., & Soto C. (2017). Delaying aging in Caenorhabditis elegans with protein aggregation inhibitors. *Biochem. Biophys. Res. Commun.* **482**(1), 62–67. PMID: 27810360; doi: 10.1016/j.bbrc.2016.10.143.
14. Ganne A., Balasubramaniam M., Griffin W.S.T., Shmookler Reis R.J., & Ayyadevara S. (2022). Glial fibrillary acidic protein: A biomarker and drug target for Alzheimer's disease. *Pharmaceutics* **14**(7). PMID: 35890250; doi: 10.3390/pharmaceutics14071354.
15. Kakraba S., Ayyadevara S., Penthala N.R., Balasubramaniam M., Ganne A., Liu L., … Shmookler Reis R.J. (2019). A novel microtubule-binding drug attenuates and reverses protein aggregation in animal models of Alzheimer's disease. *Front. Mol. Neurosci.* **12**(310). PMID: 31920540; doi: 10.3389/fnmol.2019.00310.
16. Sterniczuk R., Antle M.C., Laferla F.M., & Dyck R.H. (2010). Characterization of the 3xTg-AD mouse model of Alzheimer's disease: Part 2. Behavioral and cognitive changes. *Brain Res.* **1348**, 149–155. PMID: 20558146; doi: 10.1016/j.brainres.2010.06.011.
17. Hall A.M., & Roberson E.D. (2012). Mouse models of Alzheimer's disease. *Brain Res. Bull.* **88**(1), 3–12. PMID: 22142973; doi: 10.1016/j.brainresbull.2011.11.017.
18. Yu X., Guan P.P., Guo J.W., Wang Y., Cao L.L., Xu G.B., … Wang P. (2015). By suppressing the expression of anterior pharynx-defective-1alpha and -1beta and inhibiting the aggregation of beta-amyloid protein, magnesium ions inhibit the cognitive decline of amyloid precursor protein/presenilin 1 transgenic mice. *FASEB J.* **29**(12), 5044–5058. PMID: 26293690; doi: 10.1096/fj.15-275578.
19. Malpetti M., Kievit R.A., Passamonti L., Jones P.S., Tsvetanov K.A., Rittman T., … Rowe J.B. (2020). Microglial activation and tau burden predict cognitive decline in Alzheimer's disease. *Brain* **143**(5), 1588–1602. PMID: 32380523; doi: 10.1093/brain/awaa088.
20. Fan X., Cui L., Zeng Y., Song W., Gaur U., & Yang M. (2019). 14-3-3 proteins are on the crossroads of cancer, aging, and age-related neurodegenerative disease. *Int. J. Mol. Sci.* **20**(14). PMID: 31323761; doi: 10.3390/ijms20143518.
21. Foote M., & Zhou Y. (2012). 14-3-3 proteins in neurological disorders. *Int. J. Biochem. Mol. Biol.* **3**(2), 152–164. PMID: 22773956.
22. Gu Q., Cuevas E., Raymick J., Kanungo J., & Sarkar S. (2020). Downregulation of 14-3-3 proteins in Alzheimer's disease. *Mol. Neurobiol.* **57**(1), 32–40. PMID: 31487003; doi: 10.1007/s12035-019-01754-y.
23. Dehghani Z., Meratan A.A., Saboury A.A., & Nemat-Gorgani M. (2020). Alpha-synuclein fibrillation products trigger the release of hexokinase I from mitochondria: Protection by curcumin, and possible role in pathogenesis of Parkinson's disease. *Biochim. Biophys. Acta Biomembr.* **1862**(6), 183251. PMID: 32113849; doi: 10.1016/j.bbamem.2020.183251.
24. Mortilla M., & Sorbi S. (1990). [Hexokinase in Alzheimer's disease]. *Medicina (Firenze)* **10**(2), 168–169. PMID: 2273956.
25. Akahira J., Sugihashi Y., Suzuki T., Ito K., Niikura H., Moriya T., … Yaegashi N. (2004). Decreased expression of 14-3-3 sigma is associated with advanced disease in human epithelial ovarian cancer: its correlation with aberrant DNA methylation. *Clin. Cancer Res.* **10**(8), 2687–2693. PMID: 15102672; doi: 10.1158/1078-0432.ccr-03-0510.
26. Qi H., Lei X., Wang Y., Yu S., Liu T., Zhou S.K., … Xiao S. (2022). 14-3-3 proteins contribute to autophagy by modulating SINAT-mediated degradation of ATG13. *Plant Cell* **34**(12), 4857–4876. PMID: 36053201; doi: 10.1093/plcell/koac273.
27. Sari F.R., Watanabe K., Thandavarayan R.A., Harima M., Zhang S., Muslin A.J., … Aizawa Y. (2010). 14-3-3 protein protects against cardiac endoplasmic reticulum stress (ERS) and ERS-initiated apoptosis in experimental diabetes. *J. Pharmacol. Sci.* **113**(4), 325–334. PMID: 20644335; doi: 10.1254/jphs.10047fp.
28. An Y., Varma V.R., Varma S., Casanova R., Dammer E., Pletnikova O., … Thambisetty M. (2018). Evidence for brain glucose dysregulation in Alzheimer's disease. *Alzheimers Dement.* **14**(3), 318–329. PMID: 29055815; doi: 10.1016/j.jalz.2017.09.011.
29. Joo I.L., Lam W.W., Oakden W., Hill M.E., Koletar M.M., Morrone C.D., … Stefanovic B. (2022). Early alterations in brain glucose metabolism and vascular function in a transgenic rat model of Alzheimer's disease. *Prog. Neurobiol.* **217**, 102327. PMID: 35870681; doi: 10.1016/j.pneurobio.2022.102327.
30. Baik S.H., Ramanujan V.K., Becker C., Fett S., Underhill D.M., & Wolf A.J. (2023). Hexokinase dissociation from mitochondria promotes oligomerization of VDAC that facilitates NLRP3 inflammasome assembly and activation. *Sci. Immunol.* **8**(84), eade7652. PMID: 37327321; doi: 10.1126/sciimmunol.ade7652.
31. Han S., He Z., Jacob C., Hu X., Liang X., Xiao W., … Xie Q. (2021). Effect of increased IL-1beta on expression of HK in Alzheimer's disease. *Int. J. Mol. Sci.* **22**(3). PMID: 33525649; doi: 10.3390/ijms22031306.

32. Saraiva L.M., Seixas da Silva G.S., Galina A., da-Silva W.S., Klein W.L., Ferreira S.T., & De Felice F.G. (2010). Amyloid-beta triggers the release of neuronal hexokinase 1 from mitochondria. *PLoS One* **5**(12), e15230. PMID: 21179577; doi: 10.1371/journal.pone.0015230.

33. Magri A., Risiglione P., Caccamo A., Formicola B., Tomasello M.F., Arrigoni C., … Messina A. (2021). Small hexokinase 1 peptide against toxic SOD1 G93A mitochondrial accumulation in ALS rescues the ATP-related respiration. *Biomedicines* **9**(8). PMID: 34440152; doi: 10.3390/biomedicines9080948.

34. Johansen M.C., Ye W., Gross A., Gottesman R.F., Han D., Whitney R., … Levine D.A. (2023). Association between acute myocardial infarction and cognition. *JAMA Neurol.* **80**(7), 723–731. PMID: 37252710; doi: 10.1001/jamaneurol.2023.1331.

35. Xie W., Zheng F., Yan L., & Zhong B. (2019). Cognitive decline before and after incident coronary events. *J. Am. Coll. Cardiol.* **73**(24), 3041–3050. PMID: 31221251; doi: 10.1016/j.jacc.2019.04.019.

36. Pottle A. (2020). Prevalence and patterns of cognitive impairment in acute coronary syndrome patients: A systematic review. *Eur. J. Prev. Cardiol.* **27**(3), 281–283. PMID: 31791145; doi: 10.1177/2047487319889720.

37. Wolters F.J., Segufa R.A., Darweesh S.K.L., Bos D., Ikram M.A., Sabayan B., … Sedaghat S. (2018). Coronary heart disease, heart failure, and the risk of dementia: A systematic review and meta-analysis. *Alzheimers Dement.* **14**(11), 1493–1504. PMID: 29494808; doi: 10.1016/j.jalz.2018.01.007.

38. Nesvizhskii A.I., Keller A., Kolker E., & Aebersold R. (2003). A statistical model for identifying proteins by tandem mass spectrometry. *Anal. Chem.* **75**(17), 4646–4658. PMID: 14632076; doi: 10.1021/ac0341261.

39. Mainali N., Balasubramaniam M., Johnson J., Ayyadevara S., & Shmookler Reis R.J. (2024). Leave-one-out-analysis (LOOA): Web-based tool to predict influential proteins and interactions in aggregate-crosslinking proteomic data. *Bioinformation* **20**(1), 4–10. PMID: 38352912; doi: 10.6026/973206300200004.

40. Ganne A., Balasubramaniam M., Ayyadevara S., & Shmookler Reis R.J. (2022). Machine-learning analysis of intrinsically disordered proteins identifies key factors that contribute to neurodegeneration-related aggregation. *Front. Aging Neurosci.* **14**, 938117. PMID: 35992603; doi: 10.3389/fnagi.2022.938117.

41. Balasubramaniam M., Ganne A., Mainali N., Pahal S., Ayyadevara S., & Shmookler Reis R.J. (2024). Alzheimer's-specific brain amyloid interactome: Neural-network analysis of intra-aggregate crosslinking identifies novel drug targets. *iScience* **27**(1), 108745. PMID: 38274404; doi: 10.1016/j.isci.2023.108745.

42. Layfield R., Fergusson J., Aitken A., Lowe J., Landon M., & Mayer R.J. (1996). Neurofibrillary tangles of Alzheimer's disease brains contain 14-3-3 proteins. *Neurosci. Lett.* **209**(1), 57–60. PMID: 8734909; doi: 10.1016/0304-3940(96)12598-2.

43. Di Meco A., Curtis M.E., Lauretti E., & Pratico D. (2020). Autophagy dysfunction in Alzheimer's disease: Mechanistic insights and new therapeutic opportunities. *Biol. Psychiatry* **87**(9), 797–807. PMID: 31262433; doi: 10.1016/j.biopsych.2019.05.008.

44. Scheper W., Nijholt D.A., & Hoozemans J.J. (2011). The unfolded protein response and proteostasis in Alzheimer disease: Preferential activation of autophagy by endoplasmic reticulum stress. *Autophagy* **7**(8), 910–911. PMID: 21494086; doi: 10.4161/auto.7.8.15761.

45. Jia H., Liang Z., Zhang X., Wang J., Xu W., & Qian H. (2017). 14-3-3 proteins: An important regulator of autophagy in diseases. *Am. J. Transl. Res.* **9**(11), 4738–4746. PMID: 29218076.

46. Dosanjh L.E., Brown M.K., Rao G., Link C.D., & Luo Y. (2010). Behavioral phenotyping of a transgenic Caenorhabditis elegans expressing neuronal amyloid-beta. *J. Alzheimers Dis.* **19**(2), 681–690. PMID: 20110612; doi: 10.3233/JAD-2010-1267.

47. Collaborators GBDDF (2022). Estimation of the global prevalence of dementia in 2019 and forecasted prevalence in 2050: An analysis for the Global Burden of Disease Study 2019. *Lancet Public Health* **7**(2), e105–e125. PMID: 34998485; doi: 10.1016/S2468-2667(21)00249-8.

48. Giunta B., Fernandez F., Nikolic W.V., Obregon D., Rrapo E., Town T., & Tan J. (2008). Inflammaging as a prodrome to Alzheimer's disease. *J. Neuroinflammation* **5**, 51. PMID: 19014446; doi: 10.1186/1742-2094-5-51.

49. Faria M.C., Goncalves G.S., Rocha N.P., Moraes E.N., Bicalho M.A., Gualberto Cintra M.T., … Sousa L.P. (2014). Increased plasma levels of BDNF and inflammatory markers in Alzheimer's disease. *J. Psychiatr. Res.* **53**, 166–172. PMID: 24576746; doi: 10.1016/j.jpsychires.2014.01.019.

50. Thackeray J.T., Hupe H.C., Wang Y., Bankstahl J.P., Berding G., Ross T.L., … Bengel F.M. (2018). Myocardial inflammation predicts remodeling and neuroinflammation after myocardial infarction. *J. Am. Coll. Cardiol.* **71**(3), 263–275. PMID: 29348018; doi: 10.1016/j.jacc.2017.11.024.

51. Wang S., Luo Q., Chen H., Huang J., Li X., Wu L., … Jiang H. (2020). Light emitting diode therapy protects against myocardial ischemia/reperfusion injury through mitigating neuroinflammation. *Oxid. Med. Cell Longev.* **2020**, 9343160. PMID: 32963707; doi: 10.1155/2020/9343160.

52. Wang X., Guo Z., Ding Z., & Mehta J.L. (2018). Inflammation, autophagy, and apoptosis after myocardial infarction. *J. Am. Heart Assoc.* **7**(9). PMID: 29680826; doi: 10.1161/JAHA.117.008024.

53. Zhang W., Xiao D., Mao Q., & Xia H. (2023). Role of neuroinflammation in neurodegeneration development. *Signal Transduct. Target Ther.* **8**(1), 267. PMID: 37433768; doi: 10.1038/s41392-023-01486-5.

54. Currais A., Fischer W., Maher P., & Schubert D. (2017). Intraneuronal protein aggregation as a trigger for inflammation and neurodegeneration in the aging brain. *FASEB J.* **31**(1), 5–10. PMID: 28049155; doi: 10.1096/fj.201601184.

55. Klaips C.L., Jayaraj G.G., & Hartl F.U. (2018). Pathways of cellular proteostasis in aging and disease. *J. Cell Biol.* **217**(1), 51–63. PMID: 29127110; doi: 10.1083/jcb.201709072.

56. Li Z., Jansen M., Pierre S.R., & Figueiredo-Pereira M.E. (2003). Neurodegeneration: Linking ubiquitin/proteasome pathway impairment with inflammation. *Int. J. Biochem. Cell Biol.* **35**(5), 547–552. PMID: 12672447; doi: 10.1016/s1357-2725(02)00384-9.

57. Mainali N., Li X., Wang X., Balasubramaniam M., Ganne A., Kore R., … Ayyadevara S. (2023). Myocardial infarction elevates endoplasmic reticulum stress and protein aggregation in heart as well as brain. *Mol. Cell Biochem.* PMID: 37922111; doi: 10.1007/s11010-023-04856-3.

58. Huang N., Marie S.K., Livramento J.A., Chammas R., & Nitrini R. (2003). 14-3-3 protein in the CSF of patients with rapidly progressive dementia. *Neurology* **61**(3), 354–357. PMID: 12913197; doi: 10.1212/01.wnl.0000078890.89473.ed.

59. Mateo I., Sanchez-Juan P., Rodriguez-Rodriguez E., Infante J., Fernandez-Viadero C., Pena N., … Combarros O. (2008). 14-3-3 zeta and tau genes interactively decrease Alzheimer's disease risk. *Dement. Geriatr. Cogn. Disord.* **25**(4), 317–320. PMID: 18319590; doi: 10.1159/000119123.

60. Neal C.L., Xu J., Li P., Mori S., Yang J., Neal N.N., … Yu D. (2012). Overexpression of 14-3-3zeta in cancer cells activates PI3K via binding the p85 regulatory subunit. *Oncogene* **31**(7), 897–906. PMID: 21743495; doi: 10.1038/onc.2011.284.

61. Xu Y., Ren J., He X., Chen H., Wei T., & Feng W. (2019). YWHA/14-3-3 proteins recognize phosphorylated TFEB by a noncanonical mode for controlling TFEB cytoplasmic localization. *Autophagy* **15**(6), 1017–1030. PMID: 30653408; doi: 10.1080/15548627.2019.1569928.

62. Thandavarayan R.A., Giridharan V.V., Sari F.R., Arumugam S., Veeraveedu P.T., Pandian G.N., … Watanabe K. (2011). Depletion of 14-3-3 protein exacerbates cardiac oxidative stress, inflammation and remodeling process via modulation of MAPK/NF-kB signaling pathways after streptozotocin-induced diabetes mellitus. *Cell Physiol. Biochem.* **28**(5), 911–922. PMID: 22178943; doi: 10.1159/000335805.

63. Underwood R., Gannon M., Pathak A., Kapa N., Chandra S., Klop A., & Yacoubian T.A. (2021). 14-3-3 mitigates alpha-synuclein aggregation and toxicity in the in vivo preformed fibril model. *Acta Neuropathol. Commun.* **9**(1), 13. PMID: 33413679; doi: 10.1186/s40478-020-01110-5.

64. Foote M., Qiao H., Graham K., Wu Y., & Zhou Y. (2015). Inhibition of 14-3-3 proteins leads to schizophrenia-related behavioral phenotypes and

synaptic defects in mice. *Biol. Psychiatry* **78**(6), 386–395. PMID: 25863357; doi: 10.1016/j.biopsych.2015.02.015.

65. Shimada T., Fournier A.E., & Yamagata K. (2013). Neuroprotective function of 14-3-3 proteins in neurodegeneration. *Biomed. Res. Int.* **2013**, 564534. PMID: 24364034; doi: 10.1155/2013/564534.
66. Saiz A., Graus F., Dalmau J., Pifarre A., Marin C., & Tolosa E. (1999). Detection of 14-3-3 brain protein in the cerebrospinal fluid of patients with paraneoplastic neurological disorders. *Ann. Neurol.* **46**(5), 774–777. PMID: 10553996.
67. Dalla Y., Singh N., Jaggi A.S., Singh D., & Ghulati P. (2009). Potential of ezetimibe in memory deficits associated with dementia of Alzheimer's type in mice. *Indian J. Pharmacol.* **41**(6), 262–267. PMID: 20407557; doi: 10.4103/0253-7613.59925.
68. Yu J., Wang W.N., Matei N., Li X., Pang J.W., Mo J., … Zhang J.H. (2020). Ezetimibe attenuates oxidative stress and neuroinflammation via the AMPK/Nrf2/TXNIP pathway after MCAO in rats. *Oxid. Med. Cell Longev.* **2020**, 4717258. PMID: 31998437; doi: 10.1155/2020/4717258.